



# Separation Characteristic and Selectivity of Lithium from Geothermal Brine Using Forward Osmosis

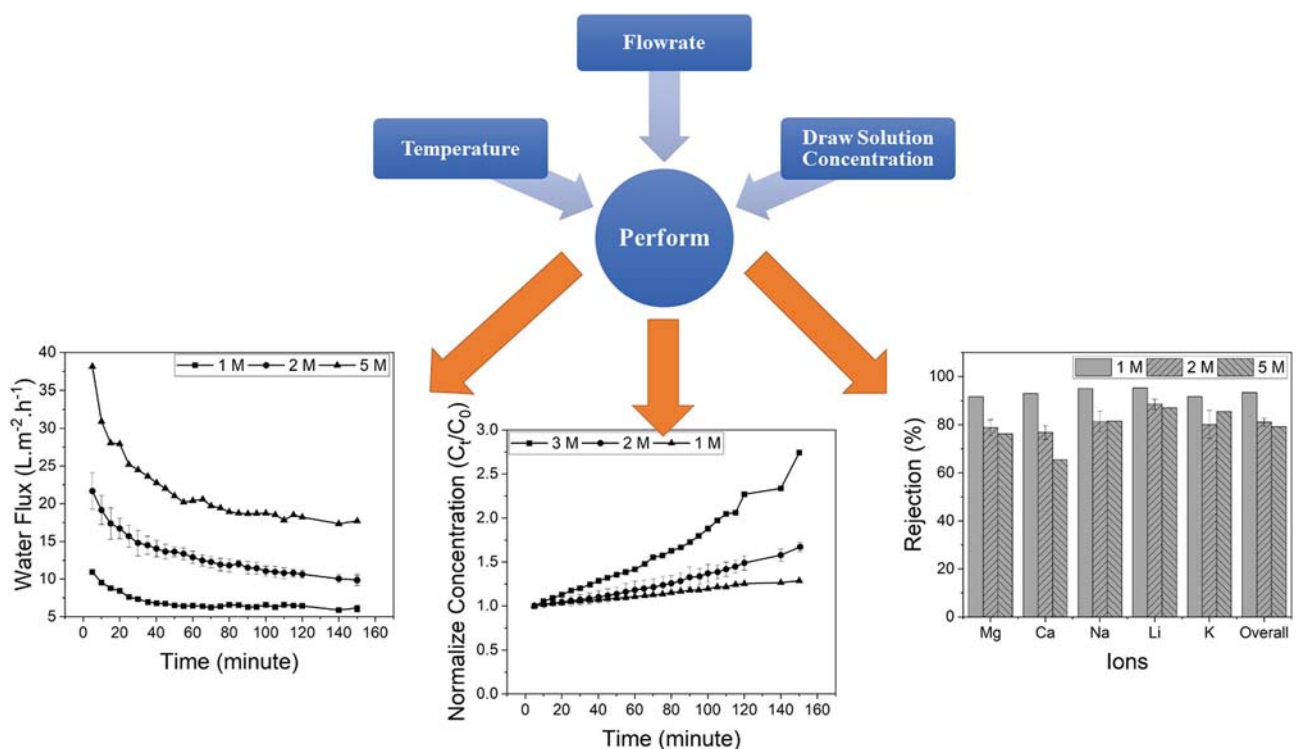
Pra Cipta Buana Wahyu Mustika<sup>1,4</sup> · Widi Astuti<sup>3</sup> · Slamet Sumardi<sup>3</sup> · Himawan Tri Bayu Murti Petrus<sup>1,2</sup> · Sutijan<sup>1</sup>

Received: 15 April 2022 / Accepted: 13 September 2022  
© The Minerals, Metals & Materials Society 2022

## Abstract

The need for lithium as a raw material for battery production in electric vehicles has triggered the growth of the lithium industry throughout the world, resulting in massive competition for the exploitation of lithium. Responding to these challenges, lithium recovery technology continues to be developed, one of which is membrane technology. This research focuses on the use of forward osmosis (FO) technology. The search for the best operating condition parameters for the process highlights a major concern. The condition parameters include temperature, draw solution concentration, and flow rate. The temperature varied from 30, 33, 36, 39 to 42 °C, the draw solution concentration varied from 1, 2 to 5 M, while the flow rate varied by 2, 3 and 4 L h<sup>-1</sup>. The best conditions were obtained at a temperature of 42 °C, a concentration of 5 M draw solution, a flow rate of 4 L h<sup>-1</sup> with a flux of 68.47 L m<sup>-2</sup> h<sup>-1</sup>, a normalized concentration ratio of 3.31, and an average solute rejection of 79.25%. Meanwhile, the most suitable osmotic pressure model to explain the phenomenon in the FO process is the Extended Pitzer.

## Graphical Abstract



The contributing editor for this article was Adam Clayton Powell.

Extended author information available on the last page of the article

**Keywords** Lithium · Battery · Green energy · Forward osmosis · Geothermal brine

## List of Symbols

$J_W$	Water flux ( $\text{L m}^{-2} \text{h}^{-1}$ )
$A$	Water permeability coefficient ( $\text{m s}^{-1} \text{atm}^{-1}$ )
$B$	Solute permeability coefficient ( $\text{m s}^{-1} \text{atm}^{-1}$ )
$\pi_D$	Osmotic pressure of draw solution (atm)
$\pi_F$	Osmotic pressure of feed solution (atm)
$\pi_{D,b}$	The osmotic pressure of the bulk draw solution (atm)
$\pi_{F,b}$	The osmotic pressure of the bulk feed solution (atm)
$S$	Membrane structural parameter (m)
$k$	Solute resistivity ( $\text{s m}^{-1}$ )
$D$	Salt diffusion coefficient ( $\text{m}^2 \text{s}^{-1}$ )
$K$	Resistance to salt transport in the porous support ( $\text{s m}^{-1}$ )
$\pi$	Osmotic pressure (atm)
$R$	Ideal gas constant ( $\text{L atm K}^{-1} \text{mol}^{-1}$ )
$C$	Concentration ( $\text{mol L}^{-1}$ )
$V$	Water molar volume ( $\text{mL mol}^{-1}$ )
$T$	Temperature (K)
$a_W$	Water activity
$M$	Molality ( $\text{mol L}^{-1}$ )
$\varnothing$	Activity coefficient
$z_x$ and $z_m$	Ionic charges
$B_{\text{mx}}(0)$ and $C_{\text{mx}}$	Solute-specific Pitzer constants
$k$	Mass transfer coefficient ( $\text{m s}^{-1}$ )
$d_h$	The hydraulic diameter of the membrane channel (m)
$Sh$	Sherwood number
$Re$	Reynolds number
$v$	The flow velocity of the solution ( $\text{m s}^{-1}$ )
$\rho$	The density of the solution ( $\text{g mL}^{-1}$ )
$Sc$	Schmidt number
$W$	Width of the membrane channel (m)
$H$	Height of the membrane channel (m)
$\mu$	Dynamic viscosity (cP)
$t$	Membrane thickness (m)
$\tau$	Membrane tortuosity
$\varepsilon$	Membrane porosity
$\nu$	Kinematic viscosity ( $\text{m}^{-2} \text{s}^{-1}$ )
RO	Reverse osmosis
FO	Forward osmosis
CTA	Cellulose Triacetate
ICP	Internal concentration polarization
ECP	External concentration polarization

## Introduction

The crisis in fossil energy resources is a significant factor in encouraging renewable energy development. Several renewable energy sources are being used intensively, including hydropower, modern biomass, geothermal, solar, wind, and seawater [1, 2]. In some cases, energy sources also have their utilization problems: geothermal mineral deposits in piping systems. The mineral deposits at PLTU Dieng Indonesia have been minimized by a precipitation process developed by Setiawan et al. [3]. Besides the potential for energy and the resulting problem of mineral deposits, geothermal brine also contains valuable minerals, including boron, lithium, and arsenic. In this case, lithium in the geothermal brine creates a potential for downstream utilization of battery loading [4].

Geothermal brine extraction and concentration techniques are the determinants of the downstream efficiency of this potential. Given these challenges, many techniques have been developed, such as nanofiltration, ion exchange, liquid–liquid extraction, adsorption, and electrodialysis (ED) [5–8]. The nanofiltration extraction technique has the main advantage of being compact (low footprint) [9, 10]. On the other hand, high operating energy and membrane fouling is still accompanying problem [11]. Other techniques, such as ED extraction, can provide high product purity (> 95%), monovalent selectivity, and are environmentally friendly [7, 12, 13]. Meanwhile, the concentration technique has not been developed much and still refers to conventional evaporation. This traditional method takes a long process, has a large evaporation area, and depends on the weather [14–16]. Several developments in membrane-based concentration techniques have been known and used for lithium recovery, including reverse osmosis (RO), membrane distillation (MD), and forward osmosis (FO) [17].

Potential exploration and development of FO as a geothermal concentration technique will be carried out in this research. Meanwhile, this potential is based on its advantages: environmentally friendly, energy-efficient, and high rejection processes. Research related to lithium concentration using FO has previously been carried out by Sun et al. [18], showing that surface modification of polyethylene membranes can improve its properties and performance. The highest performance was obtained at 0.5 M NaCl with the orientation of the active side facing the feed solution, which showed water flux and reverses salt flux, respectively:  $66.3 \text{ L m}^{-2} \text{h}^{-1}$  and  $5.25 \text{ L g}^{-1}$ . Other research has also been carried out by Pham et al. [19], using cellulose triacetate (CTA)

and thin film composite (TFC) membranes. The concentration of five times higher than the initial concentration was achieved after 30 h of processing using a thin film composite (TFC) membrane. In addition to the two researchers, Li et al. [16] also carried out research using cellulose triacetate (CTA) and thin film composite (CTA) membranes, which examined the orientation of the active side towards the draw solution-feed solution, which plays an important role in the concentration factor. The highest concentration factor was achieved with the orientation of the active side facing the feed solution and  $MgCl_2$  as the draw solution. The results showed Li and Mg, respectively: 2.3 and 2.8 times the initial concentration.

The FO movement force is a different osmotic pressure, which is an advantage in energy demand because no

hydraulic pressure is involved [20, 21]. By relying only on osmotic pressure, the transfer process takes place spontaneously. Therefore, the resulting membrane fouling value is not as high as pressurized processes such as RO, nanofiltration (NF), and so on [22]. The water transfer mechanism in FO occurs by moving some water from the feed liquid body to the draw solution liquid body through the semipermeable membrane [22, 23]. Rejection and Water flux are measurable parameters that show the performance of FO as a concentration technique. In this case, various operating parameters and their effects are reviewed. Several operating parameters have been selected in this research, including temperature, draw solution concentration, and flow rate (Table 1).

**Table 1** Technologies used for lithium recovery from various lithium resources

Membrane technology	Water resource	Performance	Reference
Reverse osmosis (Hydraulic pressure as driving force)	Industrial lithium wastewater	The research evaluates the energy consumption between the RO and ED processes. The RO operating pressure is varied between 15 and 20 bar. The RO concentration process stops when the conductivity of the solution reaches $50 \text{ mS cm}^{-1}$ . The measured energy consumption is $7.58$ and $7.81 \text{ kWh m}^{-3}$ , respectively. In addition, the average permeates flux was $14.42$ and $20.25 \text{ L m}^{-2} \text{ h}^{-1}$ , respectively	[24]
Membrane distillation (temperature different as driving force)	Synthetic brine	A combination of membrane distillation (MD) and nanofiltration (NF) was performed for lithium recovery. The NF process takes place before MD, which aims to increase the lithium concentration before processing and reduce the multivalent ion fouling on the membrane. After 140 h of operation, the solution was successfully concentrated from 100 to 1200 ppm	[16]
Forward osmosis (osmotic pressure as driving force)	Synthetic brine	The research evaluated two types of TFC and CTA membranes, and two types of draw solutions with varying concentrations of 1–5 M. Effects of concentration, membrane orientation, and pH were also evaluated. The results show that the CTA membrane has a lower reverse flux value than TFC. The final concentration of lithium in the retentate solution after 30 h of processing was $12 \text{ g L}^{-1}$	[19]
	Chaerhan salt lake brine	The research applies two types of membranes CTA and TFC. Reports show that the membrane side orientation provides lithium separation and different concentration rates. In addition, the type of draw solution was also observed in the research. The highest concentration was obtained using the CTA membrane with the orientation of the active side facing the draw solution of magnesium chloride	[25]
	Current studies	The main operating conditions are evaluated by testing variations in temperature, draw solution concentration, and flow rate. The variations in temperature and flow rate have not been carried out by previous research	

## Materials and Methods

### FO Membrane

This research used an asymmetric cellulose triacetate (CTA) membrane supplied from FTS H2O (Sterlitech) USA [26]. Meanwhile, the cellulose triacetate membrane has hydrophilic properties, which are characterized by a low contact angle ( $<90^\circ$ ) [27, 28]. Hydrophilic membranes tend to have high fouling resistance and stable flux [19]. According to a study by M.T. Pham et al. [19], the membrane has a pore size of 0.37 nm, a contact angle of  $48 \pm 2^\circ$ , and is hydrophilic, with a rejection of sodium chloride (NaCl)  $>98\%$ . The membrane has recommended operating conditions in the pH range of 2–7 with a maximum operating temperature of 50 °C.

### Feed and Draw Solution

#### Feed

Geothermal brine in this research was synthesized by dissolving several types of chloride salts into demineralized water. The composition used is presented in Table 2 as follows,

The composition refers to the real geothermal brine data approach from Dieng, Central Java, Indonesia, but does not include other components such as boron, arsenic, and silica. This research will only be oriented towards a large part of the study where the content of other impurities has been eliminated first using another process. All chemical compounds were purchased from Sigma Aldrich, the following purity: sodium chloride (NaCl, 99%), potassium chloride (KCl, 99%), magnesium chloride hexahydrate ( $\text{MgCl}_2 \cdot 6\text{H}_2\text{O}$ , 99%), calcium chloride hexahydrate ( $\text{CaCl}_2 \cdot 6\text{H}_2\text{O}$ , 99%), and lithium chloride (LiCl, 99%). Demineralized water is produced independently using a RO system, while the measured purity in total dissolved solids (TDS) is about  $\pm 5$  ppm.

**Table 2** Synthetic brine geothermal composition

Component	Concentration (ppm)
NaCl	7500
KCl	2500
$\text{MgCl}_2$	50
$\text{CaCl}_2$	400
LiCl	50

### Draw Solution

Draw solution was synthesized by dissolving a mass amount of sodium chloride (NaCl) regarding the maximum solubility in water, which is  $357 \text{ g L}^{-1}$  at 25 °C so that the variations in this research were taken below these values, including 1, 2, and 5 M. Apart from being based on the maximum solubility of sodium chloride, another reason for choosing this concentration variation is also related to the stability of the solute flux with increasing concentration of sodium chloride solution. [29, 30]. On the other hand, the effect of flow rate on flux and solute flux has been carried out. The results show that a moderate flow rate significantly reduces the formation of concentration polarization [31, 32]. The thermodynamic properties of the feed solution and draw solutions' thermodynamic properties are approximated from the Aspen Plus® data.

### FO System

The research was conducted on a laboratory scale FO cell supplied from Sterlitech with type CF042. This cell has an active area of  $42 \text{ cm}^2$  ( $3.2 \text{ in}^2$ ). Variations in operating conditions were 30, 36, and 42 °C, while the flow rates were 2, 3, and 4  $\text{L h}^{-1}$ . Based on previous research, the effect of operating temperature has a significant impact on flux and solute flux, as well as membrane structure parameters [33–35]. Moreover, attention regarding the preservation of the membrane is also taken in selecting temperature variations. Previous research by A.M. Awad et al. [37] and N. Niksefat et al. [38] only limited its operation to the 5–40 °C range. The structure of the CTA membrane, which is cellulose-based, is easy to leach when exposed to high temperatures. V. Vatanpour et al. [36] also noted that operating temperatures that are too high, around 50 °C, decrease water permeability and a non-uniform membrane size. Thus, selecting temperature variations in the operating temperature range close to the previous research reference can be used. However, analysis regarding the effect of low flow rate on the significance of concentration polarization is also the aim of this research. Meanwhile, the flow rate value variation considers fluid dynamics (laminar, turbulent, or transitional), calculated through the Reynolds number on the  $42 \text{ cm}^2$  active areas (which will be explained in the next section). The closed-loop controlled system uses two peristaltic pumps. Mass change data were collected every 5 min for 2.5 h using a digital scale. Samples before and after the process were analyzed using ICP-OES (PlasmaQuant—Model PQ 9000 Elite). Meanwhile, the concentration diagram using FO is presented in Fig. 1 as follows:

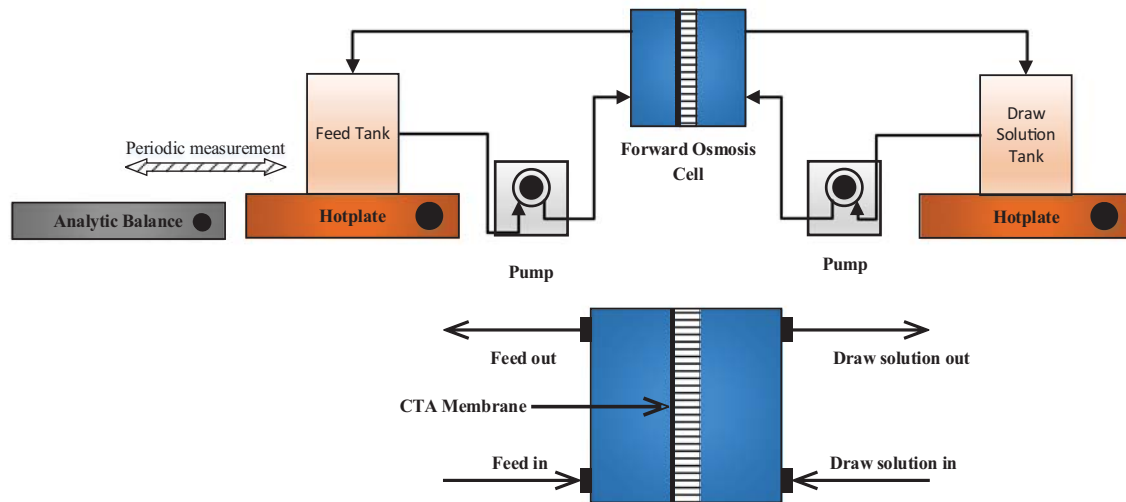


Fig. 1 Experimental apparatus for FO cell

## Theoretical Model

### Water Flux Modelling

As the driving force for the FO process, Osmosis impacts the concentration difference gradient between the bulk feed and bulk draw solution, which is the main factor for the magnitude of the resulting flux value [37, 38]. In general, Eq. (1) is commonly used to calculate the resulting flux value as follows,

$$J_W = A(\pi_D - \pi_F). \quad (1)$$

The osmotic pressure of the solution is generally denoted  $\pi$ , the index D as the draw solution, and F as the feed. The water permeability coefficient of the membrane is denoted A. The water flux model (1) does not consider the impact of concentration polarization. Thus, this model needs to be developed for more complex processes. The two main polarizations that need to be included are internal and external concentration polarization [39, 40]. The water flux model that considers the two polarizations is written in Eq. (2) as follows,

$$J_W = A \left[ \frac{\pi_{D,b} \exp\left(-\frac{J_W S}{D}\right) - \pi_{F,b} \exp\left(\frac{J_W}{k}\right)}{1 + \frac{B}{J_W} \left[ \exp\left(\frac{J_W}{K}\right) - \exp\left(-\frac{J_W S}{D}\right) \right]} \right]. \quad (2)$$

The osmotic pressure of the bulk liquid is sub-indexed as b. The mass transfer coefficient values and solute resistance are k and K, respectively. Some other symbols or notations include solute permeability coefficient (B), structural parameter (S), and diffusivity coefficient (D).

### Osmotic Pressure

Theoretically, the value of the osmotic pressure can be calculated through several approaches. The most straightforward method is Van't Hoff as Eq. (3) follows [41],

$$\pi = nCRT. \quad (3)$$

The Van't Hoff factor is denoted n, implementing the existing ionization values. The concentration of the feed solution and draw solution is denoted C, and the temperature of the solution is denoted T. In contrast, the ideal gas constant is denoted R. The application of Eq. (3) is limited to aqueous solutions. Another equation that can be used for calculating osmotic pressure is the activity model in Eq. (4) as follows,

$$\pi = -\left(\frac{RT}{V}\right) \ln(a_w). \quad (4)$$

The molar volume of the solution is denoted V, while the water activity is denoted  $a_w$  [39]. The value of  $a_w$  can be calculated using an approximation derived from the Pitzer equation for the electrolyte solution in Eq. (5) as follows,

$$a_w = \exp\left(-0.01802 \sum_i M_i\right). \quad (5)$$

The solute molality and activity coefficient are denoted  $M_i$  and  $\gamma_i$ , respectively. The value of the activity coefficient is calculated by Eq. (6–10) as follows,

$$\gamma_i - 1 = z_m z_x F + 2m \left(\frac{v_m v_x}{v}\right) B_{mx} + 2m^2 \left[\frac{(v_m v_x)^{1.5}}{v}\right] C_{mx} \quad (6)$$

$$F = -\frac{0.3921^{0.5}}{1 + 1.21^{0.5}} \quad (7)$$

$$I = 0.5 \left( \sum_i m_i z_i^2 \right) \quad (8)$$

$$|z_m z_x| = \frac{\sum_i m_i z_i^2}{\sum_i m_i} \quad (9)$$

$$B_{mx} = B_{mx}(0) + B_{mx} \exp(-2.01^{0.5}). \quad (10)$$

The ion charge is denoted  $z_x$  and  $z_m$ . The stoichiometric coefficients are denoted  $v_x$  and  $v_m$ , while the specific constants of Pitzer's solution are denoted  $B_{mx}(0)$  and  $C_{mx}$ . All calculation equations related to activity coefficients are derived from the equations obtained from Pitzer's research [42].

### Mass Transfer Coefficient

External concentration polarization (ECP) is influenced by the mass transfer coefficient value ( $k$ ). The value of this parameter is approximated by Eq. (11) as follows:

$$k = \frac{ShD}{d_h}. \quad (11)$$

The hydraulic diameter, Sherwood number, and diffusivity coefficient are denoted  $d_h$ ,  $Sh$ , and  $D$ , respectively. The hydraulic diameter ( $d_h$ ) value can be calculated through Eq. (12) as follows [43],

$$d_h = \frac{4WH}{W + H}. \quad (12)$$

The Reynold number ( $Re$ ) as the implementation of hydrodynamics in the system needs to be calculated using Eq. (13) to determine a laminar, turbulent, or transitional flow. If the value of  $Re < 2000$ , the flow is laminar, while  $Re > 4000$ , the flow is turbulent, and between the two values means transition flow.

$$Re = \frac{d_h v \rho}{\mu}. \quad (13)$$

The solution's viscosity, density, and flow viscosity are denoted by  $\mu$ ,  $\rho$ , and  $v$ . The Sherwood number ( $Sh$ ) calculation for laminar flow follows Eq. (14) as follows,

$$Sh = 1.85 \left( Re Sc \frac{d_h}{L} \right)^{0.33}, \quad (14)$$

Meanwhile, for turbulent flow, the Eq. (15) follows,

$$Sh = 1.85 Re^{0.75} Sc^{0.33}. \quad (15)$$

The Schmidt number ( $Sc$ ) in Eqs. (14) and (15) can be calculated using Eq. (16) as follows,

$$Sc = \frac{\nu}{D}, \quad (16)$$

$\nu$  in Eq. (16) is the kinematic viscosity. The equation for calculating the Reynold number ( $Re$ ), Sherwood number ( $Sh$ ), Schmidt number ( $Sc$ ) and mass transfer coefficient ( $k$ ) refers to the research of McCutcheon et al. [35, 39, 44].

### Solute Resistivity

The effect of internal concentration polarization (ICP) is influenced by the value of solute resistance [45]. The solute resistance value can be calculated through Eq. (16) as follows,

$$K = \frac{t\tau}{D\varepsilon}. \quad (17)$$

The thickness, tortuosity, and porosity of the membrane are denoted as  $t$ ,  $\tau$ , and  $\varepsilon$ .

### Diffusivity Coefficient

In this research, the effect of temperature on the diffusivity coefficient can be approximated using the Stokes–Einstein Eq. (18) as follows [46]:

$$\frac{D_{T_1}}{D_{T_2}} = \frac{T_1 \mu_{T_2}}{T_2 \mu_{T_1}}. \quad (18)$$

The diffusivity coefficients of various ions are presented in Table 3 as follows:

### Rejection

The calculation of rejection of each cation is calculated by Eq. (19), as follows:

$$\text{Rejection}(\%) = \left( 1 - \frac{C_{F,f}}{C_{F,i}} \right) \times 100, \quad (19)$$

where,  $C_{F,f}$  and  $C_{F,i}$  are the initial and final feed concentrations, respectively.

**Table 3** Diffusivity coefficient ( $D$ ) of various ions contained in the geothermal brine at a temperature of 25 °C

Ion	Mg <sup>+2</sup>	Li <sup>+</sup>	Na <sup>+</sup>	K <sup>+</sup>	Ca <sup>+2</sup>
Diffusivity coefficient ( $D$ ) ( $10^9$ m <sup>2</sup> s <sup>-1</sup> )	0.720	1.030	1.330	1.957	0.792

## Results and Discussion

### Effect of Operating Conditions

#### Effect of Temperature on Water Flux

The performance of FO is determined by the amount of water taken during the process and the rejection value that can be achieved. As for the research, the effect of operating temperature varied from 30, 33, 36, 39 to 42 °C. Meanwhile, other variables are kept constant in research related to the effect of temperature: (1) Draw solution concentration at 5 M, and (2) Flow rate at 4 L h<sup>-1</sup>. The determination of the draw solution concentration is based on considerations related to osmotic pressure as a function of concentration. This was discussed in “Materials and Methods” section, and high osmotic pressure is expected to result in high flux. Meanwhile, the determination of the flow rate is based on similar considerations. A high flow

rate decreases external concentration polarization (ECP) due to high fluid circulation.

Evaluation of the flux produced by FO with cellulose triacetate (CTA) membranes at various temperatures, as well as other constant operating conditions, is shown in Fig. 2A. Observations show that the effect of temperature is quite clearly observed for each variation, it is also shown that the tendency of flux decreases in each variation. It should be noted that various reasons can cause this decreased flux, including (1) The amount of water transferred from the bulk feed through the CTA semipermeable membrane to the bulk draw solution. This results in a decrease in the draw solution concentration, which is directly related to osmotic pressure, (2) The formation of external concentration polarization (ECP) on the membrane surface due to the gradation of the draw solution dilution on the membrane surface. If further evaluated, the flux formed due to temperature variations has a quite observable difference.

It can be observed in Table 4 that the highest water flux under these conditions was 38.16 L m<sup>-2</sup> h<sup>-1</sup> at 42 °C.

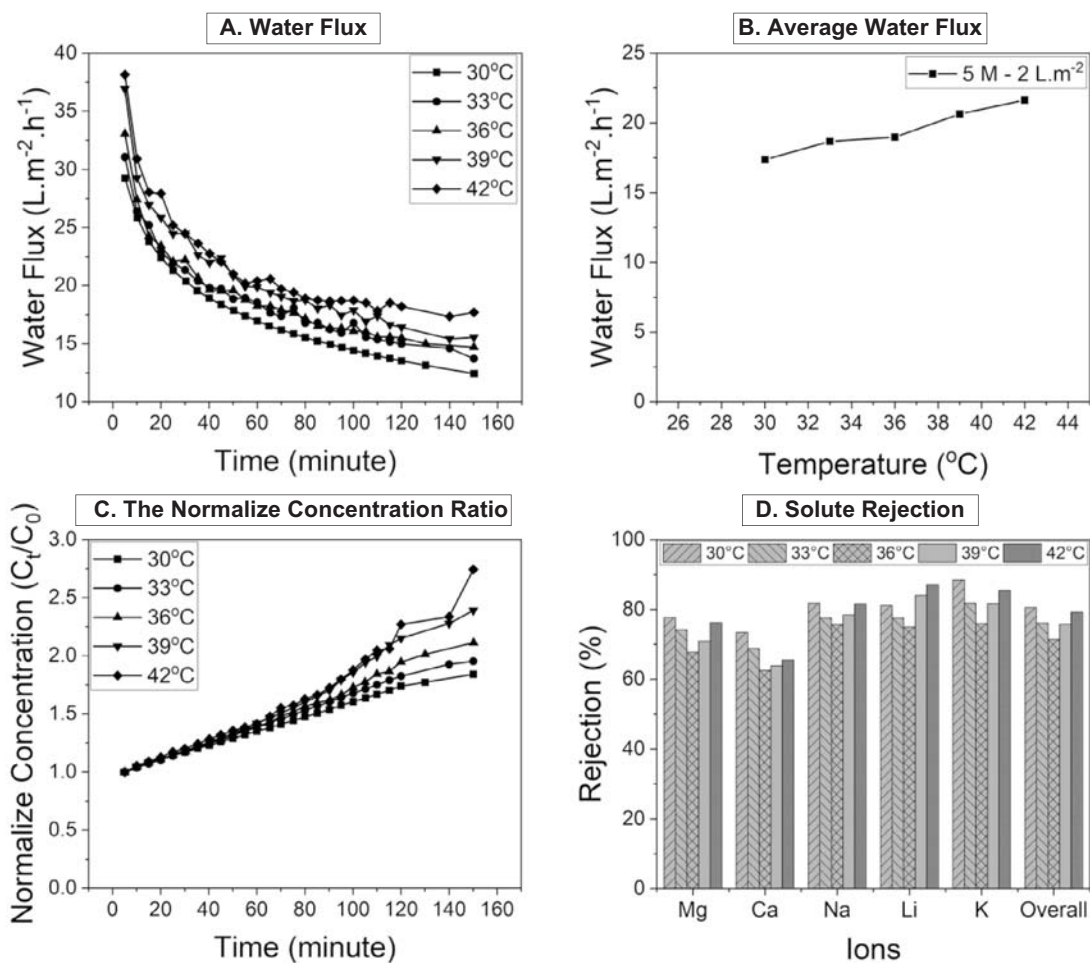


Fig. 2 Effect of various temperatures: **A** Water Flux, **B** average water flux, **C** the normalised concentration ratio, **D** solute rejection

**Table 4** Water flux at various temperatures, at a concentration of 5 M and a flow rate: 2 L h<sup>-1</sup>

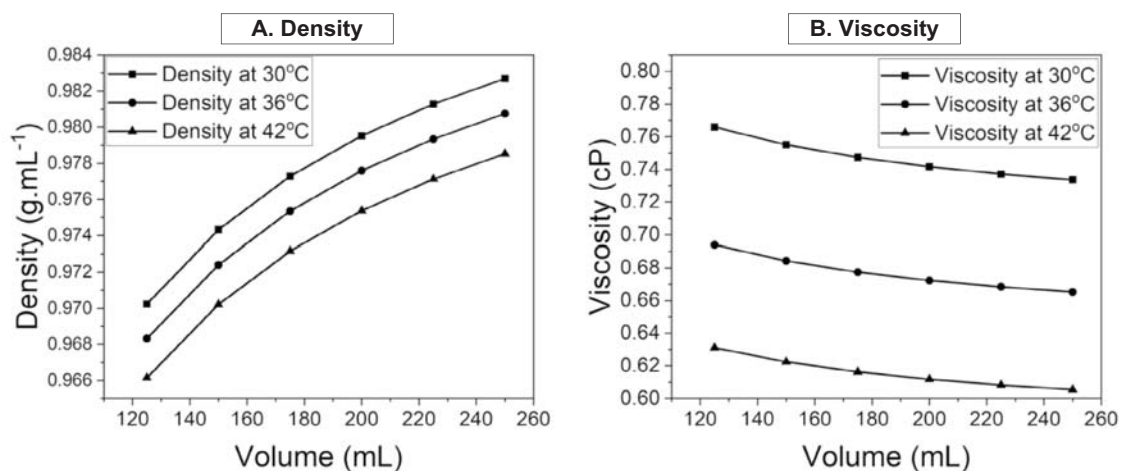
Temperature (30 °C)	30	33	36	39	42
Initial (L m <sup>-2</sup> h <sup>-1</sup> )	29.25	31.06	33.07	36.91	38.16
Final (L m <sup>-2</sup> h <sup>-1</sup> )	12.43	13.72	14.72	15.55	17.71

Generally, the influence of temperature on flux cannot be independent. Several factors are related to the feed solution's properties and draw solution, including osmotic pressure, diffusivity coefficient, density, viscosity, and so on [34]. Mathematically and linearly, the view of increasing osmotic pressure as a function of temperature can be observed from Eqs. (3) and (4). Thus, an increase in temperature inevitably increases osmotic pressure. The observations also prove that at high temperatures, the flux is also high, and vice versa (see Fig. 2A, B). Thus, the effect of temperature on the osmotic pressure gradient between the draw solution and the feed solution, which is the driving force of FO, is one of the critical processes. On another note, the draw solution concentration is much higher than the feed solution, so it becomes a more dominant factor. The dominance factor is related to the direction of displacement and the driving force that arises due to differences in osmotic pressure. Based on the solubility properties of chloride salts, the solution has a positive enthalpy. An increase in temperature tends to increase the solubility of the salt so that the osmotic pressure increases, which increases the resulting water flux [47].

Apart from affecting osmotic pressure, the viscosity of the solution also plays a significant role in increasing the water flux that can be achieved. Based on the hypothesis put forward by Phuntsho et al. [34], it is stated that the lower viscosity of the draw solution has an impact on increasing the rate of water transfer through the membrane support

layer, thereby reducing the effect of internal concentration polarization (ICP) [34]. In this research, the effect of viscosity is not directly carried out in the laboratory but through a theoretical approach using Aspen Plus®. The approach shows that the effect of temperature on viscosity is quite significant. On another note, the transfer of water only occurs from the feed solution to the draw solution, so the viscosity of the feed solution is quite representative. In addition, in the approach process using Aspen Plus® there are several notes or/and assumptions, including: (1) Changes in the concentration of dissolved ions in the feed solution are considered to have no significant effect on the density or viscosity because the feed concentration is relatively dilute [48], (2) Select the equation of state (EOS) electrolyte nonrandom two liquid (eNRTL), (3) The approach due to changes in feed volume from the beginning to the end of the process (250 → 125 mL) can be represented. The results of the approach using Aspen Plus® for density and viscosity can be seen in Fig. 3 as follows.

The Stokes–Einstein approach appraised ion diffusivity's effect as a temperature function (Eq. 18). From these equations, it is shown that the effect of temperature also plays a direct role in the diffusivity and indirectly on the viscosity that has been mentioned previously. Increasing temperature affects the diffusivity value, at which a higher temperature will increase the diffusivity. The increase in the diffusivity value is expected to reduce the resistance in the support layer, reducing the effect of internal concentration polarization (ICP). A thorough evaluation of flux can be done by looking at the flux trend on average. In this case, the average flux is obtained by the simple moving average method, which is the sum of all fluxes for each data collection time divided by the number of data. The overall results showed that water flux at 42 °C was the highest, 39, 36, 33 and 30 °C. Comparing the average flux as a function of

**Fig. 3** A Density and B viscosity as a function of volume at various temperatures



temperature, it is observed that the increase in temperature in the range of 30–42 °C produces a fairly linear gradient of increasing flux. This can be observed in Fig. 2B. From the trend presented in Fig. 2B, the increase in flux with temperature changes has a behaviour that is in line with flux at various times for each temperature variation. This trend of change in average flux is linear with temperature change and supports the related fact that flux is proportional to the change in osmotic pressure, which is directly a function of temperature (Eqs. 3 and 4).

The water flux value achieved during the process will affect the concentration rate of the geothermal brine solution using the FO process. This effect is presented in Fig. 2C, which displays the ratio of concentration rates expressed in normalized concentrations at various times. Therefore, the relation that states that temperature changes will affect the normalized concentration can be determined (as opposed to flux). The best conditions are obtained at a temperature of 42 °C followed by a temperature of 39, 36, 33 and 30 °C, as shown in Fig. 2C. The highest value at 42 °C was reached in the range of 2.74, while the lowest was at 30 °C with 1.84. In detail, the normalized concentration in each variation has a similar pattern, but at 42 °C, temperature variations show quite different behaviour at 120–150 min. This is possible because, at the time of data collection, the homogeneity of the feed solution has not been achieved, so the concentration has not implemented the overall concentration of the solution.

The solute rejection value was also observed for its effect on changes in operating temperature. At the same time, the results are presented in Fig. 2D. As discussed in the previous section, an increase in ionic diffusivity can occur due to an increase in temperature. Therefore, ion migration across a semipermeable membrane is possible. Figure 2D shows that the ions can diffuse across a semipermeable membrane. However, the ability to diffuse is not the only reason ions can move across the membrane. The low viscosity of water due to an increase in temperature also encourages the dissolved ions to move along with the water flux. The size of the ions passing through the membrane is essential in achieving solute rejection. The ion size of the solution system is known as the hydrated ion radius. In Table 5, the hydration radius ( $r_h$ ) and hydration enthalpy ( $\Delta G$ ) of various ions contained in geothermal brine at a temperature of 25 °C is observed as follows [49, 50],

Research by Yamaguchi et al. [51] has shown an increase in solution temperature impacts decreasing the ionic radius of hydration. Besides impacting the ionic hydration radius, the temperature increase also impacts the membrane's pore size due to the swelling phenomenon in the polymer making up the membrane. As for the increasing temperature, the membrane experiences swelling in the constituent polymer chains, resulting in a widening pore size [52]. These effects

**Table 5** Hydration ionic radius ( $r_h$ ) and hydration enthalpy ( $\Delta G$ ) of various ions contained in the geothermal brine at a temperature of 25 °C

Ion	Li <sup>+</sup>	Na <sup>+</sup>	K <sup>+</sup>	Mg <sup>2+</sup>	Ca <sup>2+</sup>
Hydration radius ( $r_h$ ) (nm)	0.382	0.358	0.331	0.428	0.412
Hydration enthalpy ( $\Delta G$ ) (kJ mol <sup>-1</sup> )	- 519	- 409	- 322	- 1921	- 1577

make it easier for the ions to move through the membrane. In this research, the distribution of hydration pore size ( $r_h$ ) has not been determined with certainty, but according to the literature, the hydrated pore size of the CTA membrane will range from 0.300 to 0.348 nm [53]. Previous research conducted by Pham et al. [19] showed that the CTA membrane had a hydration pore size ( $r_h$ ) of 0.370 nm.

The results presented in Fig. 2D have not shown the phenomenon of decreasing solute rejection due to increased temperature. Further observations found an anomaly at 42 °C, indicating that the overall ion rejection was higher than 36 °C. It is possible that at 42 °C, the swelling of the membrane is already at its maximum limit, while the ions' hydration radius is widening due to the loosening of the molecular bonds of water rather than ions. This causes the ions to not move across the membrane even though other factors, such as the viscosity of the solution, decrease.

According to Tansel et al. [48, 54], water molecules will experience stronger bonds to ions with small sizes than large ones. Therefore, the hydration enthalpy indicates the hydration bond strength (Table 5). If based only on the enthalpy of hydration, the first hydration shell of the row: Mg<sup>2+</sup> > Ca<sup>2+</sup> > Li<sup>+</sup> > Na<sup>+</sup> > K<sup>+</sup>. However, research data show different results, so other factors must be considered as the basis for the rejection of monovalent (K<sup>+</sup>, Na<sup>+</sup>, Li<sup>+</sup>) higher than divalent (Mg<sup>2+</sup> and Ca<sup>2+</sup>). In contrast to the research conducted by Coday et al. [55], which showed that monovalent and divalent rejected more than 90%, specifically Mg<sup>2+</sup> was close to 100%.

Meanwhile, this indicates that the research results obtained have anomalies due to certain things, possibly due to interactions between monovalent ions. This interaction has been described in research conducted by Zangi [56], which alludes to the effect of charge density ions (ex: Cl<sup>-</sup>, I<sup>-</sup>, Li<sup>+</sup>, Na<sup>+</sup>) on water molecules. The presence of water is considered a bridge between ions to interact with each other, which can be formed when these ions form hydrogen bonds with water. However, this analogy does not fully represent the phenomenon that occurs for the dominant ions (Na<sup>+</sup> and K<sup>+</sup>). The mechanism for the formation of the hydration layer

begins with the attraction of oxygen by positive ions, resulting in the attraction of hydrogen. The presence of hydrogen will form a skin that will bind to oxygen from other structures [48]. Overall, the solute rejection results ranged from 71.41 to 80.53%. Potassium ( $K^+$ ) has the highest rejection value, ranging from 75.95 to 88.47%, while the lowest value is occupied by  $Ca^{2+}$ , with a value of 62.61–73.45%.

#### Effect of Draw Solution Concentration on Water Flux

The effect of the draw solution concentration in this research was determined by varying the concentrations of 1, 2, and 5 M, respectively. The operation occurs at a temperature of 42 °C and a flow rate of 2 L h<sup>-1</sup>. The results showed that the 5 M concentration produced the highest water flux with a 38.16 L m<sup>-2</sup> h<sup>-1</sup>. The comparison of the results of the concentration variation is presented in Fig. 4A.

The effect of increasing the concentration can be observed in Fig. 4A, which shows that increasing the concentration of the draw solution results in an increase in water flux. This phenomenon occurs because the change in the ionic activity value of the draw solution has increased. When comparing the effect of increasing temperature, a more significant result is obtained by varying the concentration of the draw solution. This is because ionic mobility in solution tends to be more limited, resulting in easier collisions between ions. The average water flux is presented in Fig. 4B.

At various concentrations, the increase in water flux is proportional to the increase in the concentration of the draw solution. This will affect the concentration rate of the geothermal brine solution that can be achieved during the process. If observed, the increasing average water flux gradient due to increasing concentration does not form a linear model for increasing concentration. This condition also proves that changes in concentration have a more significant impact than

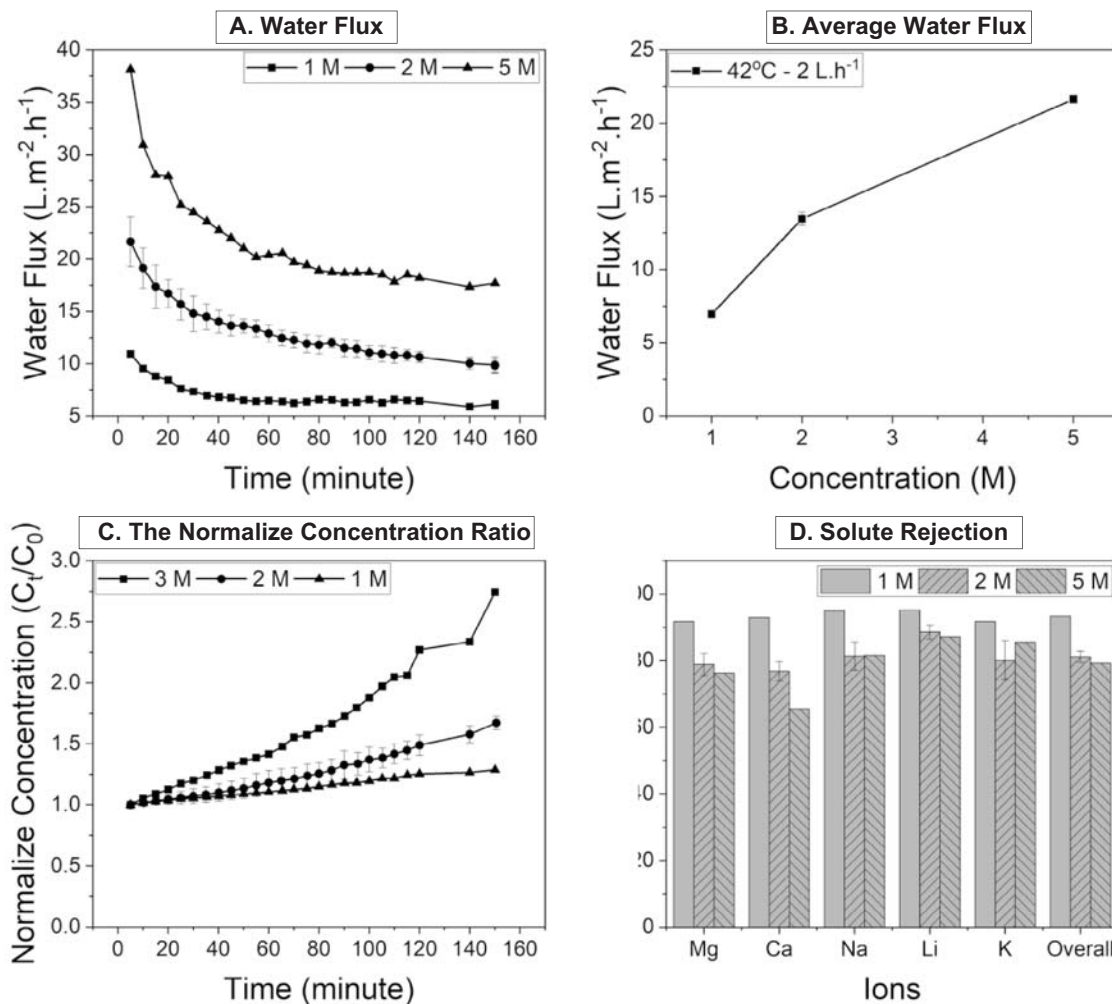


**Fig. 4** Effect of various draw solution concentrations: **A** Water flux, **B** average water flux, **C** the normalised concentration ratio, **D** solute rejection

temperature changes. Another process performance review is carried out by considering the concentration rate (Fig. 4C). The comparison of the normalized concentration ratios presented in Fig. 4C shows that increasing the concentration of the draw solution results in an increase in the normalized concentration that can be achieved. The highest value was obtained at the 5 M draw solution concentration in the range of 2.74, while the lowest was obtained at 1 M with a value of 1.29.

The solute rejection value is used to determine the concentration performance due to variations in the concentration of the draw solution. The results of the comparison of solute rejection at various variations in the concentration of the draw solution are presented in Fig. 4D. The effect of the concentration of the draw solution on solute rejection cannot be separated from the amount of water flux produced. The extensive water flux results in the tendency for concentration polarization to form on the active surface of the membrane facing the feed. This concentration polarization increases the chances of its transfer by diffusion on the membrane surface. This is evidenced by the research results in Fig. 4D. It was observed that the 5 M variation of the draw solution produced smaller solute rejection compared to 2 and 1 M. Overall, it appears that the rejection decreased along with the increase in the draw solution concentration. However, at Na and K, deviations were found. Meanwhile, the average deviation between the two is around  $\pm 5\%$ . The best value of solute rejection is occupied by variation 1 M with 93.36%.

### Effect of Flow Rate on Water Flux

The effect of flow rate in the FO process was determined by comparing several flow rate variations, namely 2, 3, and 4 L h<sup>-1</sup>. The effect can be seen from the water flux's value, concentration rate, and rejection. The following are the results of the flow rate variations carried out at a 5 M draw solution concentration at 42 °C:

The results presented in Fig. 5A show that the influence of the flow rate on the FO process is quite different from one another at the beginning of the process. Still, over time the resulting flow rate becomes more uniform. This is possible because the membrane's concentration polarisation phenomenon was not formed at the beginning of the process, so water can easily move from the feed side to the draw solution. However, the concentration polarization began to form on the membrane surface over time. The results of the comparison of the average water flux as a function of the variation in flow rate are presented in Fig. 5B.

The research results presented in Fig. 5C show that the increase in the process flow rate is not very influential compared to other variations (temperature and draw solution concentration). This is evidenced by increasing the flow rate from 2 to 4 L h<sup>-1</sup> does not significantly differ. This

condition is related to the hydrodynamics of the solution on the membrane surface, which has not been able to eliminate the influence of the external concentration polarization formed so that water diffusion on the active surface of the membrane is still blocked by the layer formed on the membrane surface. The cross-flow configuration mechanism plays a role in the hydrodynamic system. Meanwhile, previous studies have proved that FO configuration plays a role in the hydrodynamics of the fluid on the membrane surface [57]. The study compared the cross-flow configurations of spiral wound forward osmosis (SWFO) and flat sheet forward osmosis (FSFO), and it appears that the membrane parameters (e.g. A, B, S) are different from each other.

Figure 5D presents the effect of flow rate on ion rejection. The rejection at the flow rate variation of 2 L h<sup>-1</sup> appears to be the highest. Theoretically, increasing the flow rate results in a decrease in concentration polarization, leading to high rejection. However, in this research, there is no agreement with this theory. This condition is evident in the research results in Fig. 5C. It is observed that the variation of 4 L h<sup>-1</sup> produces minor solute rejection than 3 and 2 L h<sup>-1</sup>. The highest solute rejection value was obtained at a flow rate of 2 L h<sup>-1</sup> with 93.36%. This condition occurs because an increase in the flow rate also impacts the mobility of ions through the membrane [48]. This is related to a higher shear force with an increased flow rate. Thus, ions can release hydrated water in the presence of high shear forces to move across the membrane. Conversely, the tendency to lose hydrating water on the ion surface will be small [48]. The loss of hydrating water on the ion surface makes it easier for ions to pass through the membrane pores.

### Evaluation of Parameters and Models

The variation of several parameters showed that the effect of temperature, concentration, and the process flow rate was quite significant. Related to this, the process parameters need to be evaluated. A suitable model is expected to accurately predict the water flux during the FO process. Meanwhile, a comprehensive model considers the effect of external and internal concentration polarization (ECP and ICP) (Eq. 2). In this regard, the van der Waals osmotic pressure (VDW) model (Eq. 3) and extended Pitzer (EP) (Eqs. 4–10) were used.

### Temperature Variation Model

The effect of temperature on water flux, rejection, and concentration rate has been discussed previously. An increased operating temperature increases water flux and the concentration rate. The factors that cause this phenomenon need to be analysed, including the effect of the osmotic pressure value and its suitability to the phenomenon. The results of

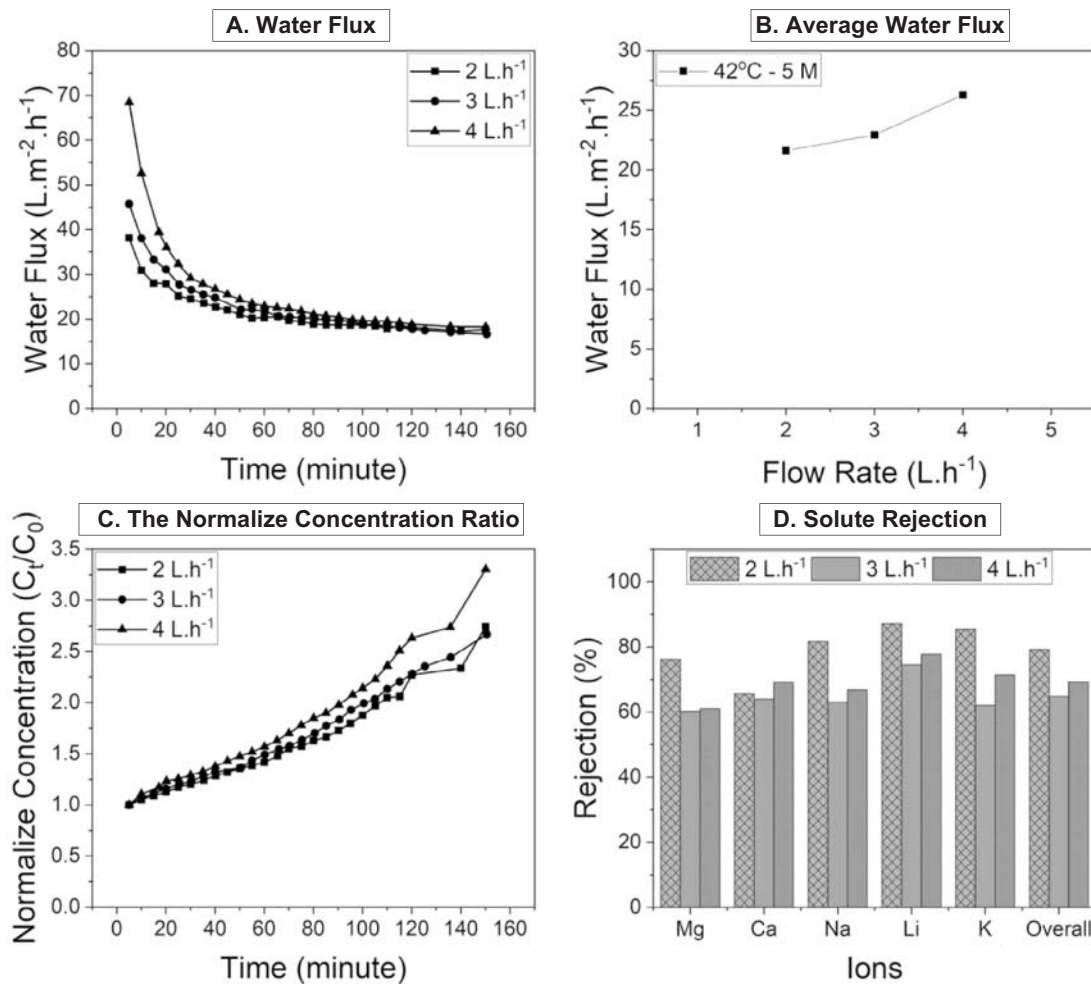


**Fig. 5** Effect of various flow rates: **A** Water flux, **B** average water flux, **C** the normalised concentration ratio, **D** solute rejection

comparing several activity models for calculating osmotic pressure as a function of temperature variations are presented in Fig. 6A.

The results presented in Fig. 6A show that the Van der Waals (VDW) and Extended Pitzer (EP) osmotic pressure models can be used in water flux modelling. Evaluation of model accuracy is assessed through statistical methods. The coefficient of determination ( $r^2$ ) between the EP and VDW models was 0.994 and 0.986, respectively. Based on these values, the EP model is more representative than the VDW model. The average value of parameters A and B from the EP model is  $0.2141 \times 10^{-7}$  and  $0.005 \times 10^{-7}$ . Besides affecting molecular and ionic interactions in solution, an increase in temperature also affects the phenomena on the membrane surface. The increase in temperature results in increased diffusion of water in the membrane. This significantly decreases the ECP value due to increasing the mass transfer coefficient value (k). Increasing water diffusion decreases solute resistance (K), significantly reducing the ICP value [39]. Research

from Yong et al. [30] and Field et al. [58] also explains the relationship between the mass transfer in the membrane and the resistance and structural parameters formed.

#### Concentration Variation Model

The results of qualitative analysis on the effect of concentration variations have been described previously, which show significant differences in water flux, rejection, and concentration rate. In the previous explanation, it was known that an increase in the concentration of the draw solution increased water flux and concentration rate and a decrease in rejection. Quantitative analysis of this phenomenon must be conducted to determine the effect of the activity model used in calculating the osmotic pressure on the FO process parameters, A and B, on the resulting water flux. The comparison in Fig. 6A shows that the EP model provides the best approximation value ( $r^2=0.992$ ). The average value of the A and B parameters from the EP model is  $0.3728 \times 10^{-7}$  and

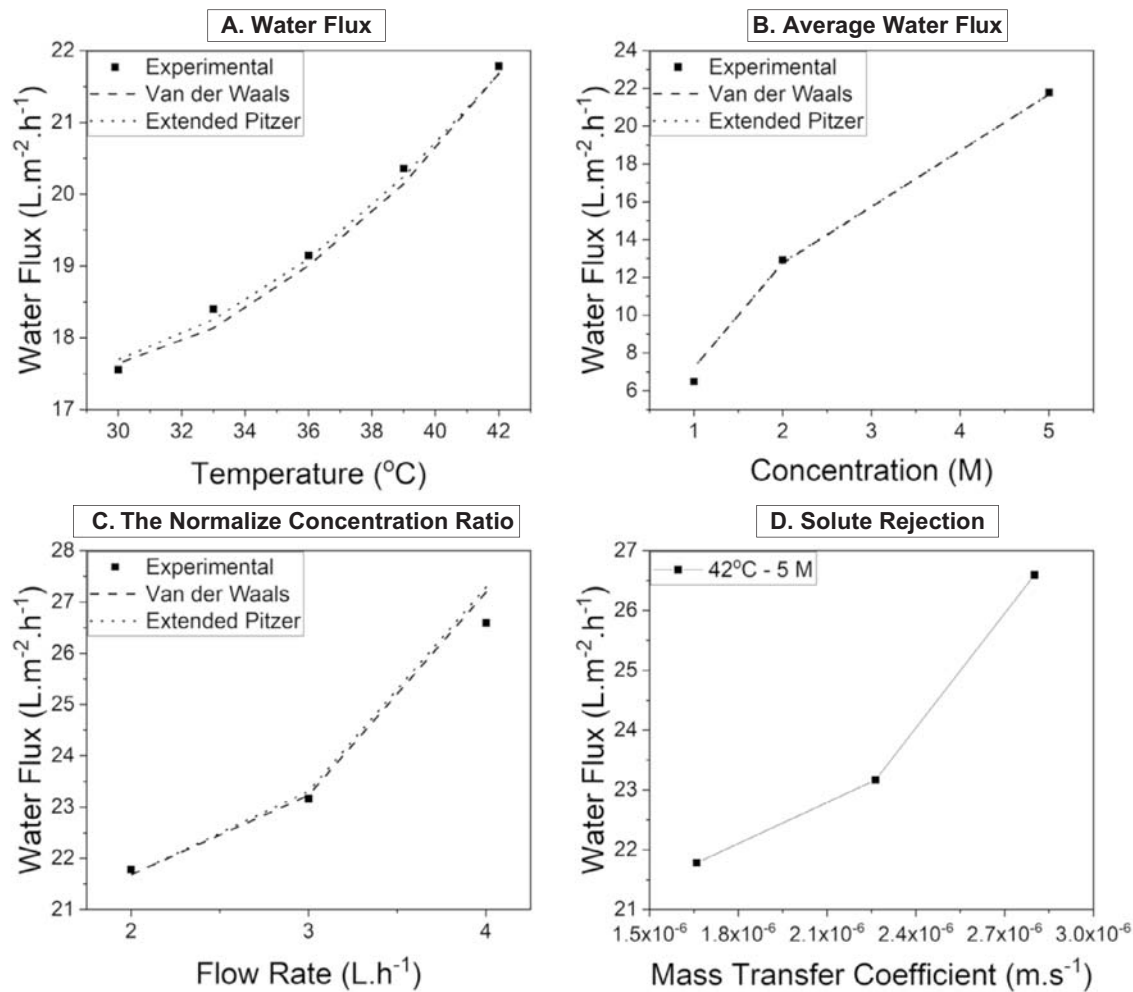


**Fig. 6** Comparison of the resulting osmotic pressure model to the resulting water flux: **A** Temperature, **B** concentration, **C** flow rate, **D** mass transfer coefficient as a function flow rate

$0.005 \times 10^{-7}$ , respectively. These parameter values indicate that the increase in water flux due to the increased concentration of the draw solution is closely related to the molecular and ionic activities in the solution. Solutions with high concentrations tend to produce high collision interactions between molecules, ions, and ions so that the activity of the solution increases. As the molecular activity increases, the draw solution's osmotic pressure increases, thereby increasing the driving force. This is already implied from the osmotic pressure model in Eqs. (3) and (4).

### Flow Rate Variation Model

The effect of process flow rate has been previously described. The results show that an increase in flow rate increases water flux and concentration rate and decreases rejection generated during the process. These conditions

indicate that the effect of changes in flow rate needs to be analyzed. As for the FO process, the increase in flow rate affects the hydrodynamics on the membrane surface, which is related to the ability of water to move from the feed to the draw solution. This ability is expressed in the mass transfer coefficient ( $k$ ). The effect of the mass transfer coefficient ( $k$ ) can be seen in Fig. 6D. The increase in water flux is closely related to the mass transfer coefficient ( $k$ ) value, observed in Fig. 6D. The comparison results in Fig. 6C show that the increase in the EP model ( $r^2 = 0.998$ ) has better compatibility with the experimental water flux model than VDW. Theoretically, it has been explained that the VDW method does not consider the ionic activity as a determinant of osmotic pressure and vice versa; EP considers it. Thus, experimental and theoretical results are coherent.

## Product Characteristics

The results of ICP analysis on the feed solution after the FO process can implement the concentration that the process can achieve. It is important to obtain this data to determine the maximum limit of lithium concentration that can be achieved. The final lithium concentration at the best conditions in this research was measured at a temperature of 42 °C, a concentration of 5 M, and a flow rate of 4 L h<sup>-1</sup>. The lithium concentrate yield reached  $\pm 120.21$  ppm or almost three times more concentrated than the feed used. While the yields for other ions, including potassium, sodium, calcium, and magnesium, are 1993.85, 5264.86, 160.10, and 332.27 ppm, respectively. Lithium concentrations are still low in industrial applications and cannot be processed further. In future research, developing a sustainable draw solution that can form high osmotic pressure is necessary. In addition, research on membrane synthesis with high rejection and selectivity needs to be developed. It is planned that the extraction of lithium from the concentrate will be carried out using an ED process, which has shown high selectivity. This is done when the synthetic brine geothermal solution has been concentrated to the expected value. The minimum lithium concentration needed to achieve 60–80% recovery in the precipitation process is 20–30 g L<sup>-1</sup> [59].

## Conclusion

The research conclusion confirms that various parameters have been evaluated for their effect on the lithium concentration process using FO. These parameters affect the flux, rate of concentration, and rejection. Draw solution concentration showed the most significant effect compared to temperature and flow rate. In addition, tests at a predetermined operating temperature range showed a theoretical increase in osmotic pressure as a function of temperature, although it was not significant. Rejection can be achieved by more than 70% for all ions, which has the potential for further expansion to increase selectivity even more. The analysis of the osmotic pressure model between the extended Pitzer (EP) and van der Waals (VDW) shows that both models can be used to approximate the selected operating condition range. Still, it is also emphasized that the extended Pitzer model is more appropriate.

**Acknowledgements** The authors are grateful for the support of Gadjah Mada University, MF Kedaireka with contract number 180/E1/KS.06.02/2022; 5975/UN1.P/Dit-PUI/HK.08.00/2022 and the collaboration of the National Research and Innovation Agency (BRIN) Lampung in this research.

## Declarations

**Conflict of interest** The authors declare that they have no conflict of interest.

## References

- Panwar NL, Kaushik SC, Kothari S (2011) Role of renewable energy sources in environmental protection: a review. *Renew Sustain Energy Rev* 15:1513–1524. <https://doi.org/10.1016/j.rser.2010.11.037>
- Yang XJ, Hu H, Tan T, Li J (2016) China's renewable energy goals by 2050. *Environ Dev* 20:83–90. <https://doi.org/10.1016/j.envdev.2016.10.001>
- Setiawan FA, Rahayuningsih E, Petrus HTBM et al (2019) Kinetics of silica precipitation in geothermal brine with seeds addition: minimizing silica scaling in a cold re-injection system. *Geotherm Energy*. <https://doi.org/10.1186/s40517-019-0138-3>
- Sujoto VSH, Sutijan AW et al (2021) Lithium recovery from synthetic geothermal brine using electro dialysis method. *IOP Conf Ser Earth Environ Sci*. <https://doi.org/10.1088/1755-1315/882/1/012003>
- Castino F, Bookhagen B, Strecker MR (2017) Rainfall variability and trends of the past six decades (1950–2014) in the subtropical NW Argentine Andes. *Clim Dyn* 48:1049–1067. <https://doi.org/10.1007/s00382-016-3127-2>
- Li L, Deshmane VG, Paranthaman MP et al (2018) Lithium recovery from aqueous resources and batteries: a brief review. *Johnson Matthey Technol Rev* 62:161–176. <https://doi.org/10.1595/205651317X696676>
- Sujoto VSH, Sutijan AW et al (2022) Effect of operating conditions on lithium recovery from synthetic geothermal brine using electro dialysis method. *J Sustain Metall* 8:274–287. <https://doi.org/10.1007/s40831-021-00488-3>
- Kim E, Patel R (2021) A review on lithium recovery by membrane process. *Membr J* 31:315–326. [https://doi.org/10.14579/membrane\\_journal.2021.31.5.315](https://doi.org/10.14579/membrane_journal.2021.31.5.315)
- Li X, Zhang C, Zhang S et al (2015) Preparation and characterization of positively charged polyamide composite nanofiltration hollow fibre membrane for lithium and magnesium separation. *Desalination* 369:26–36. <https://doi.org/10.1016/j.desal.2015.04.027>
- Sun SY, Cai LJ, Nie XY et al (2015) Separation of magnesium and lithium from brine using a Desal nanofiltration membrane. *J Water Process Eng* 7:210–217. <https://doi.org/10.1016/j.jwpe.2015.06.012>
- He CW, Wang H, Wang LC et al (2021) Fouling identification for nanofiltration membrane and the potential reduction of pollutants in the leachate by using Fe/Al/PAC coagulation. *Sustain* 13:1–12. <https://doi.org/10.3390/su13031114>
- Hoshino T (2013) Development of technology for recovering lithium from seawater by electro dialysis using ionic liquid membrane. *Fusion Eng Des* 88:2956–2959. <https://doi.org/10.1016/j.fusengdes.2013.06.009>
- Hoshino T (2015) Innovative lithium recovery technique from seawater by using world-first dialysis with a lithium ionic superconductor. *Desalination* 359:59–63. <https://doi.org/10.1016/j.desal.2014.12.018>
- Flexer V, Baspineiro CF, Galli CI (2018) Lithium recovery from brines: a vital raw material for green energies with a potential environmental impact in its mining and processing. *Sci Total Environ* 639:1188–1204. <https://doi.org/10.1016/j.scitotenv.2018.05.223>

15. Mustika P, Petrus HTBM, Sutijan S (2021) Pengaruh Kondisi Operasi Proses Pemekatan Geothermal Brine menggunakan Forward Osmosis (FO) dengan Larutan Natrium Klorida Sebagai Draw Solution. Gadjah Mada University
16. Park SH, Kim JH, Moon SJ et al (2020) Lithium recovery from artificial brine using energy-efficient membrane distillation and nanofiltration. *J Memb Sci* 598:117683. <https://doi.org/10.1016/j.memsci.2019.117683>
17. Xu S, Song J, Bi Q et al (2021) Extraction of lithium from Chinese salt-lake brines by membranes: design and practice. *J Memb Sci* 635:119441. <https://doi.org/10.1016/j.memsci.2021.119441>
18. Sun N, Dou P, Zhai W et al (2022) Polyethylene separator supported thin-film composite forward osmosis membranes for concentrating lithium enriched brine. *Water Res* 216:118297. <https://doi.org/10.1016/j.watres.2022.118297>
19. Pham MT, Nishihama S, Yoshizuka K (2020) Concentration of lithium by forward osmosis. *Hydrometallurgy* 197:105485. <https://doi.org/10.1016/j.hydromet.2020.105485>
20. Gao Y, Fang Z, Chen C et al (2020) Evaluating the performance of inorganic draw solution concentrations in an anaerobic forward osmosis membrane bioreactor for real municipal sewage treatment. *Bioresour Technol* 307:123254. <https://doi.org/10.1016/j.biortech.2020.123254>
21. Cath TY, Childress AE, Elimelech M (2006) Forward osmosis: principles, applications, and recent developments. *J Memb Sci* 281:70–87. <https://doi.org/10.1016/j.memsci.2006.05.048>
22. Blandin G, Ferrari F, Lesage G et al (2020) Forward osmosis as concentration process: review of opportunities and challenges. *Membranes (Basel)* 10:1–40. <https://doi.org/10.3390/membranes10100284>
23. Cath TY, Elimelech M, McCutcheon JR et al (2013) Standard methodology for evaluating membrane performance in osmotically driven membrane processes. *Desalination* 312:31–38. <https://doi.org/10.1016/j.desal.2012.07.005>
24. Qiu Y, Ruan H, Tang C et al (2019) Study on recovering high-concentration lithium salt from lithium-containing wastewater using a hybrid reverse osmosis (RO)-electrodialysis (ED) process. *ACS Sustain Chem Eng* 7:13481–13490. <https://doi.org/10.1021/acssuschemeng.9b03108>
25. Li J, Wang M, Zhao Y et al (2018) Enrichment of lithium from salt lake brine by forward osmosis. *R Soc Open Sci*. <https://doi.org/10.1098/rsos.180965>
26. Goh PS, Ismail AF, Ng BC, Abdullah MS (2019) Recent progresses of forward osmosis membranes formulation and design for wastewater treatment. *Water (Switzerland)*. <https://doi.org/10.3390/w11102043>
27. Zhang S, Wang KY, Chung TS et al (2010) Well-constructed cellulose acetate membranes for forward osmosis: minimized internal concentration polarization with an ultra-thin selective layer. *J Memb Sci* 360:522–535. <https://doi.org/10.1016/j.memsci.2010.05.056>
28. Nguyen TPN, Yun ET, Kim IC, Kwon YN (2013) Preparation of cellulose triacetate/cellulose acetate (CTA/CA)-based membranes for forward osmosis. *J Memb Sci* 433:49–59. <https://doi.org/10.1016/j.memsci.2013.01.027>
29. Phillip WA, Yong JS, Elimelech M (2010) Reverse draw solute permeation in forward osmosis: modeling and experiments. *Environ Sci Technol* 44:5170–5176. <https://doi.org/10.1021/es100901n>
30. Yong JS, Phillip WA, Elimelech M (2012) Coupled reverse draw solute permeation and water flux in forward osmosis with neutral draw solutes. *J Memb Sci* 392–393:9–17. <https://doi.org/10.1016/j.memsci.2011.11.020>
31. Gulied M, Al Momani F, Khraisheh M et al (2019) Influence of draw solution type and properties on the performance of forward osmosis process: energy consumption and sustainable water reuse. *Chemosphere* 233:234–244. <https://doi.org/10.1016/j.chemosphere.2019.05.241>
32. Hawari AH, Kamal N, Altaee A (2016) Combined influence of temperature and flow rate of feeds on the performance of forward osmosis. *Desalination* 398:98–105. <https://doi.org/10.1016/j.desal.2016.07.023>
33. Xie M, Price WE, Nghiem LD, Elimelech M (2013) Effects of feed and draw solution temperature and transmembrane temperature difference on the rejection of trace organic contaminants by forward osmosis. *J Memb Sci* 438:57–64. <https://doi.org/10.1016/j.memsci.2013.03.031>
34. Phuntsho S, Vigneswaran S, Kandasamy J et al (2012) Influence of temperature and temperature difference in the performance of forward osmosis desalination process. *J Memb Sci* 415–416:734–744. <https://doi.org/10.1016/j.memsci.2012.05.065>
35. Mccutcheon JR, Mcginnis RL, Elimelech M (2006) Desalination by ammonia—carbon dioxide forward osmosis: influence of draw and feed solution concentrations on process performance. *J Memb Sci* 278:114–123. <https://doi.org/10.1016/j.memsci.2005.10.048>
36. Vatanpour V, Pasaoglu ME, Barzegar H et al (2022) Cellulose acetate in fabrication of polymeric membranes: a review. *Chemosphere*. <https://doi.org/10.1016/j.chemosphere.2022.133914>
37. Monjezi AA, Mahood HB, Campbell AN (2017) Regeneration of dimethyl ether as a draw solute in forward osmosis by utilising thermal energy from a solar pond. *Desalination* 415:104–114. <https://doi.org/10.1016/j.desal.2017.03.034>
38. Bin DN, Alkhudhiri A, AlAlawi A et al (2020) Experimental investigation of forward osmosis process for boron removal from water. *J Water Process Eng* 38:101570. <https://doi.org/10.1016/j.jwpe.2020.101570>
39. Khraisheh M, Dawas N, Nasser MS et al (2020) Osmotic pressure estimation using the Pitzer equation for forward osmosis modelling. *Environ Technol (United Kingdom)* 41:2533–2545. <https://doi.org/10.1080/09593330.2019.1575476>
40. Phuntsho S, Hong S, Elimelech M, Kyong H (2014) Osmotic equilibrium in the forward osmosis process: modelling, experiments and implications for process performance. *J Memb Sci* 453:240–252. <https://doi.org/10.1016/j.memsci.2013.11.009>
41. Johnson DJ, Suwaileh WA, Mohammed AW, Hilal N (2018) Osmotic’s potential: an overview of draw solutes for forward osmosis. *Desalination* 434:100–120. <https://doi.org/10.1016/j.desal.2017.09.017>
42. Pitzer KS (1973) Thermodynamics of electrolytes. I. Theoretical basis and general equations. *J Phys Chem* 77:268–277. <https://doi.org/10.1021/j100621a026>
43. D’Haese AKH, De Leersnyder I, Vermeir P, Verliefe ARD (2018) On negative rejection of uncharged organic solutes in forward osmosis. *J Memb Sci* 548:22–31. <https://doi.org/10.1016/j.memsci.2017.11.002>
44. Mccutcheon JR, Elimelech M (2006) Influence of concentrative and dilutive internal concentration polarization on flux behavior in forward osmosis. *J Memb Sci* 284:237–247. <https://doi.org/10.1016/j.memsci.2006.07.049>
45. Bhinder A, Shabani S, Sadrzadeh M (2018) Effect of internal and external concentration polarizations on the performance of forward osmosis process. *Osmotically Driven Membr Process*. <https://doi.org/10.5772/intechopen.71343>
46. Zwanzig R, Harrison AK (1985) Modifications of the Stokes-Einstein formula. *J Chem Phys* 83:5861–5862. <https://doi.org/10.1063/1.449616>
47. Kim AS, Kim H (2017) Membrane thermodynamics for osmotic phenomena. In: Yonar T (ed) *Desalination*. InTech, London
48. Tansel B, Sager J, Rector T et al (2006) Significance of hydrated radius and hydration shells on ionic permeability during nanofiltration in dead end and cross flow modes. *Sep Purif Technol* 51:40–47. <https://doi.org/10.1016/j.seppur.2005.12.020>

49. Zhao LM, Chen QB, Ji ZY et al (2018) Separating and recovering lithium from brines using selective-electrodialysis: sensitivity to temperature. *Chem Eng Res Des* 140:116–127. <https://doi.org/10.1016/j.cherd.2018.10.009>
50. Mohammad M, Lisiecki M, Liang K et al (2020) Metal-Phenolic network and metal-organic framework composite membrane for lithium ion extraction. *Appl Mater Today*. <https://doi.org/10.1016/j.apmt.2020.100884>
51. Yamaguchi T, Ohzono H, Yamagami M et al (2010) Ion hydration in aqueous solutions of lithium chloride, nickel chloride, and caesium chloride in ambient to supercritical water. *J Mol Liq* 153:2–8. <https://doi.org/10.1016/j.molliq.2009.10.012>
52. Roy Y, Warsinger DM, Lienhard JH (2017) Effect of temperature on ion transport in nanofiltration membranes: diffusion, convection and electromigration. *Desalination* 420:241–257. <https://doi.org/10.1016/j.desal.2017.07.020>
53. Kim SJ, Kook S, O'Rourke BE et al (2017) Characterization of pore size distribution (PSD) in cellulose triacetate (CTA) and polyamide (PA) thin active layers by positron annihilation lifetime spectroscopy (PALS) and fractional rejection (FR) method. *J Memb Sci* 527:143–151. <https://doi.org/10.1016/j.memsci.2016.12.064>
54. Tansel B (2012) Significance of thermodynamic and physical characteristics on permeation of ions during membrane separation: hydrated radius, hydration free energy and viscous effects. *Sep Purif Technol* 86:119–126. <https://doi.org/10.1016/j.seppur.2011.10.033>
55. Coday BD, Heil DM, Xu P, Cath TY (2013) Effects of transmembrane hydraulic pressure on the performance of forward osmosis membranes. *Environ Sci Technol* 47:2386–2393. <https://doi.org/10.1021/es304519p>
56. Zangi R (2012) Attraction between like-charged monovalent ions. *J Chem Phys*. <https://doi.org/10.1063/1.4705692>
57. Im SJ, Jeong S, Jang A (2018) Feasibility evaluation of element scale forward osmosis for direct connection with reverse osmosis. *J Memb Sci* 549:366–376. <https://doi.org/10.1016/j.memsci.2017.12.027>
58. Field RW, Arsalan F, Ang P, Jie J (2018) Analysis of the influence of module construction upon forward osmosis performance. *Desalination* 431:151–156. <https://doi.org/10.1016/j.desal.2017.09.003>
59. An JW, Kang DJ, Tran KT et al (2012) Recovery of lithium from Uyuni salar brine. *Hydrometallurgy* 117–118:64–70. <https://doi.org/10.1016/j.hydromet.2012.02.008>

**Publisher's Note** Springer Nature remains neutral with regard to jurisdictional claims in published maps and institutional affiliations.

## Authors and Affiliations

Pra Cipta Buana Wahyu Mustika<sup>1,4</sup> · Widi Astuti<sup>3</sup> · Slamet Sumardi<sup>3</sup> · Himawan Tri Bayu Murti Petrus<sup>1,2</sup>  · Sutijan<sup>1</sup>

✉ Himawan Tri Bayu Murti Petrus  
bayupetrus@ugm.ac.id

✉ Sutijan  
sutijan@ugm.ac.id

<sup>1</sup> Chemical Engineering Department (Sustainable Mineral Processing Research Group), Faculty of Engineering, Universitas Gadjah Mada, Jl. Grafika No.2, Kampus UGM, Yogyakarta 55281, Indonesia

<sup>2</sup> Faculty of Engineering, Unconventional Geo-Resources Research Center, UGM, Jl. Grafika No.2, Kampus UGM, Yogyakarta 55281, Indonesia


<sup>3</sup> Research Center for Mining Technology, National Research and Innovation Agency (BRIN), Jl. Ir. Sutami Km. 15, Tanjung Bintang, Lampung Selatan, Lampung 35361, Indonesia

<sup>4</sup> Chemical Engineering Department, Faculty of Engineering, Universitas Surabaya, Jl. Raya Kalirungkut, Surabaya 60293, Indonesia



# Journal of Sustainable Metallurgy



 Springer  
www.springer.com  
1614-7546

**TMS**  
The Minerals, Metals & Society Institute



## **Journal of Sustainable Metallurgy**

Publishing model: Hybrid

[← Back to Overview](#)

# TMS

## **Editors**

### **Editors-in-Chief**

Kazuki Morita, *The University of Tokyo, Japan*

Uday Pal, *Boston University, United States*

Akbar Rhamdhani, *Swinburne University of Technology, Australia*

### **Founding Editors**

Diran Apelian, *Worcester Polytechnic Institute, United States*

Bart Blanpain, *KU Leuven, Belgium*

Shin-ya Kitamura, *Tohoku University, Japan*

### **Managing Editor**

Yiannis Pontikes, *KU Leuven, Belgium*

### **Editorial Oversight Committee**

Diran Apelian, *University of California, Irvine, CA, USA*

Claire Davis, *The University of Warwick, Coventry, UK*

Peter Hayes, *The University of Queensland, St Lucia, QLD, Australia*

Toru Okabe, *The University of Tokyo, Tokyo, Japan*

Dierk Raabe, *Max-Planck Institute, Dusseldorf, Germany*

## Associate Editors

Mansoor Barati, *University of Toronto, Canada*

João António Labrincha Batista, *University of Aveiro, Portugal*

Nikhil Dhawan, *Indian Institute of Technology Roorkee, India*

Sharif Jahanshahi, *Meta-Logical Solutions Ltd, Australia; University of New South Wales, Australia*

Hojong Kim, *The Pennsylvania State University, United States*

Christina Meskers, *SINTEF, Norway*

Grace Ofori-Sarpong, *University of Mines and Technology, Ghana*

Adam Powell, *Worcester Polytechnic Institute, United States*

Markus Reuter, *SMS Group GmbH, Germany; Curtin University, Australia*

Veena Sahajwalla, *University New South Wales, Australia*

Atsushi Shibayama, *Akita University, Japan*

Il Sohn, *Yonsei University, South Korea*

Zhi Sun, *Chinese Academy of Sciences, China*

Hiromichi Takebe, *Ehime University, Japan*

Yongxiang Yang, *Delft University of Technology, The Netherlands*

Zhongwei Zhao, *Central South University, China*

Hongmin Zhu, *Tohoku University, Japan*

## For authors

[Submission guidelines](#)



[Language editing services](#)



[Ethics and disclosures](#)





## Journal of Sustainable Metallurgy

Publishing model: Hybrid

[← Back to Overview](#)

# TMS

[Search all Journal of Sustainable Metallurgy articles →](#)

## Volume 8, Issue 4

December 2022

46 articles in this issue

### Sustainability of Valuable Metals Recovery from Hazardous Industrial Solid Wastes: The Role of Mechanical Activation



Review Article | 09 September 2022 | Pages: 1393 – 1421

### SPRINGER NATURE

Join our user research database & earn rewards.

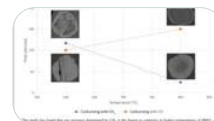
To improve your experience with our products, we need your input! Participate in User Research by signing up for our research programme.

[Join our Database](#)[No Thanks](#)

A Review on Stabilization of Ladle Furnace Slag – Powdering Issue

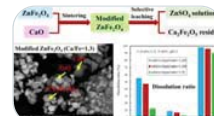


## Effect of Temperature and Gas Mixtures on Cementite Formation During the Carburization of Hydrogen-Reduced DRI



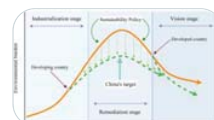
Review Article | 05 October 2022 | Pages: 1450 – 1464

## Selective Leaching of Zn from ZnFe<sub>2</sub>O<sub>4</sub> Modified by CaO in the H<sub>2</sub>SO<sub>4</sub> Solution



Short Communication | 26 August 2022 | Pages: 1465 – 1471

## The Development Scenarios and Environmental Impacts of China's Aluminum Industry: Implications of Import and Export Transition



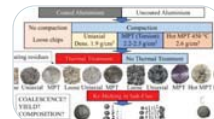
Thematic Section: REWAS 2022: Developing Tomorrow's Technical Cycles | 29 August 2022 | Pages: 1472 – 1484



Part of 1 collection:

REWAS 2022: Developing Tomorrow's Technical Cycles

## Thermal De-coating Pre-treatment for Loose or Compacted Aluminum Scrap and Consequences for Salt-Flux Recycling



Thematic Section: REWAS 2022: Developing Tomorrow's Technical Cycles | Open access | 28 October 2022 | Pages: 1485 – 1497



Part of 1 collection:

REWAS 2022: Developing Tomorrow's Technical Cycles

**SPRINGER NATURE**

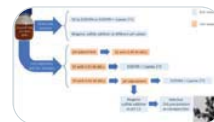
Join our user research database & earn rewards.

To improve your experience with our products, we need your input! Participate in User Research by signing up for our research programme.

Join our Database

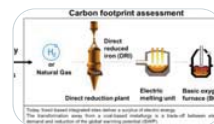
No Thanks

**Zinc Recovery from an Extreme Copper-Free Acid Mine Drainage: Studying the Prior Separation of Ferric Iron by Solvent Extraction using AliCy and/or Alkalinization**



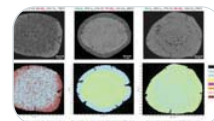
Research Article | 29 August 2022 | Pages: 1509 – 1531

**Carbon Footprint and Energy Transformation Analysis of Steel Produced via a Direct Reduction Plant with an Integrated Electric Melting Unit**



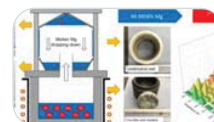
Research Article | Open access | 31 August 2022 | Pages: 1532 – 1545

**Carburization Behavior of Hydrogen-Reduced DRI Using Synthetic Bio-syngas Mixtures as Fossil-Free Carbon Sources**



Research Article | 02 September 2022 | Pages: 1546 – 1560

**The Separation Behavior of Impurities in the Purification of High-Purity Magnesium via Vacuum Distillation**



Research Article | Open access | 06 September 2022 | Pages: 1561 – 1572

**Evaluation of Functional, Microstructural, Environmental Impact, and Economic Performance of Concrete Utilizing Ferrochrome Ash and Slag**



Research Article | 06 September 2022 | Pages: 1573 – 1589

**Effect of B<sub>2</sub>O<sub>3</sub> on the Liquidus Temperature and Phase Equilibria in**



**SPRINGER NATURE**

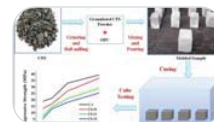
Join our user research database & earn rewards.

To improve your experience with our products, we need your input! Participate in User Research by signing up for our research programme.

Join our Database

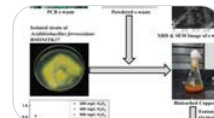
No Thanks

## Effect of Cupola Furnace Slag Addition on the Characteristics of Ordinary Portland Cement Blocks



Research Article | 13 September 2022 | Pages: 1606 - 1616

## Non-ferrous Fenton's Oxidation of Ametryn Using Bioleached E-waste Copper as a Catalyst



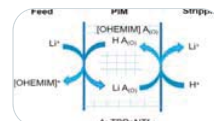
Research Article | 13 September 2022 | Pages: 1617 - 1627

## Mineralogical Characteristics and Oxygen Pressure Acid Leaching of Low-Grade Polymetallic Complex Chalcopyrite



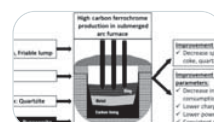
Research Article | 14 September 2022 | Pages: 1628 - 1638

## Extraction of Lithium from Brine with a High Mg/Li Ratio Using Polymer Inclusion Membrane Containing Tri-*n*-butyl Phosphate and Ionic Liquid



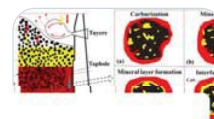
Research Article | 15 September 2022 | Pages: 1639 - 1649

## Characterization of Chromiferous Pyroxenite and Its Application as Flux in Ferrochrome Production Through an Industrial-Scale Submerged Arc Furnace



Research Article | 21 September 2022 | Pages: 1650 - 1661

## Phase and Reaction Behavior of the Iron-Coke Interface Along the Coke-Free Area in a Dissected Blast Furnace Hearth



**SPRINGER NATURE**

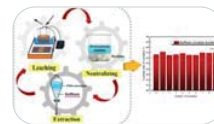
Join our user research database & earn rewards.

To improve your experience with our products, we need your input! Participate in User Research by signing up for our research programme.

Join our Database

No Thanks

**Sustainability Assessment of Recycling Leaching Closed-Loop Processes for Black Shale Raffinate and Intensive Examination of Crux Factors Including Fluoride and Heavy Metals**



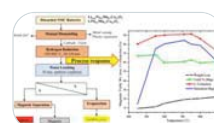
Research Article | 28 September 2022 | Pages: 1675 – 1686

**Characterization of Calcination Process of Electric Arc Furnace Dust with Lime: A Behavior of Zinc, Lead, and Iron**



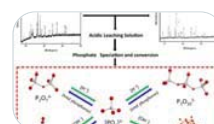
Research Article | 28 September 2022 | Pages: 1687 – 1703

**Investigation of Hydrogen Reduction for Metal Recovery from End-of-Life Lithium-Ion Batteries**



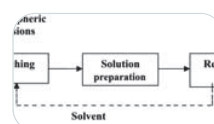
Research Article | 29 September 2022 | Pages: 1704 – 1718

**Speciation and Conversion of Metastable Phosphate in the Acidic Leaching Solution of Converter Vanadium Slag**



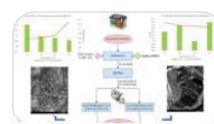
Research Article | 05 October 2022 | Pages: 1719 – 1726

**Oxidative Leaching of Akpugo Kaolinite for Alumina Recovery and Kinetic Modeling**



Research Article | 05 October 2022 | Pages: 1727 – 1743

**Lead Electrorefining Process from Exhausted Lead Acid Batteries by Using Acidic and Alkaline Electrolytes**



**SPRINGER NATURE**

Join our user research database & earn rewards.

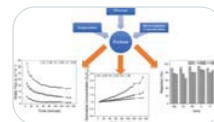
To improve your experience with our products, we need your input! Participate in User Research by signing up for our research programme.

Join our Database

No Thanks

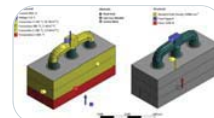


## Separation Characteristic and Selectivity of Lithium from Geothermal Brine Using Forward Osmosis



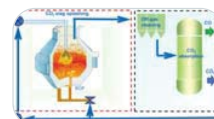
Research Article | 12 October 2022 | Pages: 1769 – 1784

## Thermo-mechanical Studies of Thimble Geometry and Stub Materials for Voltage Drop Across the Anode-Rod Connection in Aluminum Electrolysis Cell



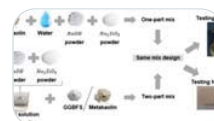
Research Article | 12 October 2022 | Pages: 1785 – 1802

## The Behavior of CO<sub>2</sub> Supersonic Jets in the Converter Slag-Splashing Process



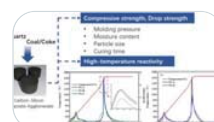
Research Article | 12 October 2022 | Pages: 1803 – 1815

## Comparison of One-Part and Two-Part Alkali-Activated Metakaolin and Blast Furnace Slag



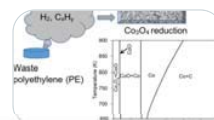
Research Article | Open access | 13 October 2022 | Pages: 1816 – 1830

## Study on Agglomeration Conditions and Reactivity of Carbon-Silicon Composite Agglomerate



Research Article | 18 October 2022 | Pages: 1831 – 1840

## Co<sub>3</sub>O<sub>4</sub> Reduction Behavior in the Gas Atmosphere Generated by Waste Polyethylene Pyrolysis: Effects of Temperature, Time, Heating Rate and Reactant Ratio



**SPRINGER NATURE**

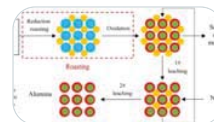
Join our user research database & earn rewards.

To improve your experience with our products, we need your input! Participate in User Research by signing up for our research programme.

Join our Database

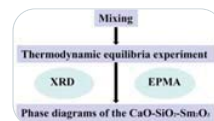
No Thanks

## The Alkaline Leaching Behavior of Silica Solid Solutions in the Product Obtained by Roasting the Mixture of High-Alumina Coal Gangue and Hematite



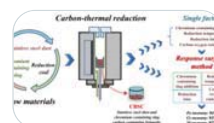
Research Article | 26 October 2022 | Pages: 1853 – 1865

## Phase Relations of the CaO–SiO<sub>2</sub>–Sm<sub>2</sub>O<sub>3</sub> System



Research Article | 28 October 2022 | Pages: 1866 – 1876

## Efficient Utilization of Stainless Steel Dust and Chromium-Containing Slag by Carbothermal Direct Reduction: Synergistic Mechanism and Optimization Analysis



Research Article | 31 October 2022 | Pages: 1877 – 1891

## Utilization of Furnace Slag for Pigments Production



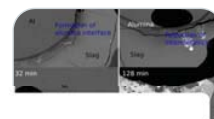
Research Article | 31 October 2022 | Pages: 1892 – 1903

## Characterization of Mined Metals from a Brazilian Sanitary Landfill



Research Article | 04 November 2022 | Pages: 1904 – 1914

## Utilization of Scrap Metals as Reductants for Improved Ni and Cu Recoveries in Copper Smelting



**SPRINGER NATURE**

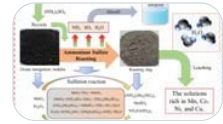
Join our user research database & earn rewards.

To improve your experience with our products, we need your input! Participate in User Research by signing up for our research programme.

Join our Database

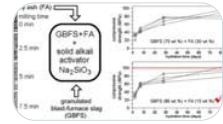
No Thanks

## A Sustainable Low-Temperature Roasting and Water Leaching Process for Simultaneously Extracting Mn, Cu, Co, and Ni from Ocean Manganese Nodules



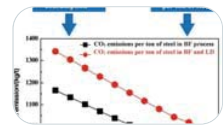
Research Article | 15 November 2022 | Pages: 1948 – 1960

## Effect of Mass Ratio and Milling on Compressive Strength and Corrosion Resistance of Blast-Furnace Slag/Fly Ash Geopolymer Activated by Solid Alkali Activator



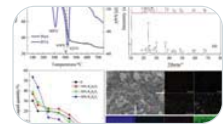
Research Article | 21 November 2022 | Pages: 1961 – 1974

## Effect of Converter Scrap Ratio on Carbon Emission in BF-LD Process



Research Article | 22 November 2022 | Pages: 1975 – 1987

## Recovery of Vanadium, Titanium, and Iron from Vanadium Titanomagnetite Concentrate Through Ammonium Sulfate Cascade Roasting with Potassium Pyrosulfate



Research Article | 22 November 2022 | Pages: 1988 – 2000

## Modeling and Analysis of Copper, Iron, and Cobalt Recovery in a Hybrid Sulfuric Acid–Sodium Chloride Media Using Artificial Neural Network



Research Article | 23 November 2022 | Pages: 2001 – 2014

## Digestion of Waste $\text{Co}_2\text{O}_3$ Using Sulfuric Acid Curing and Dissolution



**SPRINGER NATURE**

Join our user research database & earn rewards.

To improve your experience with our products, we need your input! Participate in User Research by signing up for our research programme.

Join our Database

No Thanks



## Language quality checker

[Get your manuscript edited for free →](#)

[Use our pre-submission checklist →](#)

Avoid common mistakes on your manuscript.



[This journal's calls for papers →](#)

Collections this journal is participating in.



[Sign up for alerts →](#)



## SPRINGER NATURE

Join our user research database & earn rewards.

To improve your experience with our products, we need your input! Participate in User Research by signing up for our research programme.

[Join our Database](#)

[No Thanks](#)

## **SPRINGER NATURE**

Join our user research database & earn rewards.

To improve your experience with our products, we need your input! Participate in User Research by signing up for our research programme.

[Join our Database](#)

[No Thanks](#)

## Journal of Sustainable Metallurgy

COUNTRY	SUBJECT AREA AND CATEGORY	PUBLISHER	H-INDEX
Switzerland  Universities and research institutions in Switzerland  Media Ranking in Switzerland	<a href="#">Engineering</a> <a href="#">Mechanics of Materials</a> <a href="#">Environmental Science</a> <a href="#">Environmental Science (miscellaneous)</a> <a href="#">Materials Science</a> <a href="#">Metals and Alloys</a>	<a href="#">Springer International Publishing AG</a>	<b>31</b>
PUBLICATION TYPE	ISSN	COVERAGE	INFORMATION
Journals	21993823, 21993831	2015-2022	<a href="#">Homepage</a> <a href="#">How to publish in this journal</a>

### SCOPE






Journal of Sustainable Metallurgy is a peer-reviewed journal dedicated to presenting metallurgical processes and related research aimed at improving the sustainability of metal-producing industries, with a particular emphasis on materials recovery, reuse, and recycling. Its editorial scope encompasses new techniques, as well as optimization of existing processes, including utilization, treatment, and management of metallurgically generated residues. Articles on non-technical barriers and drivers that can affect sustainability will also be considered. The journal aspires to contribute to advancing the science but also to be a catalyst for tangible change toward more sustainable practices in the metallurgical industrial sector.

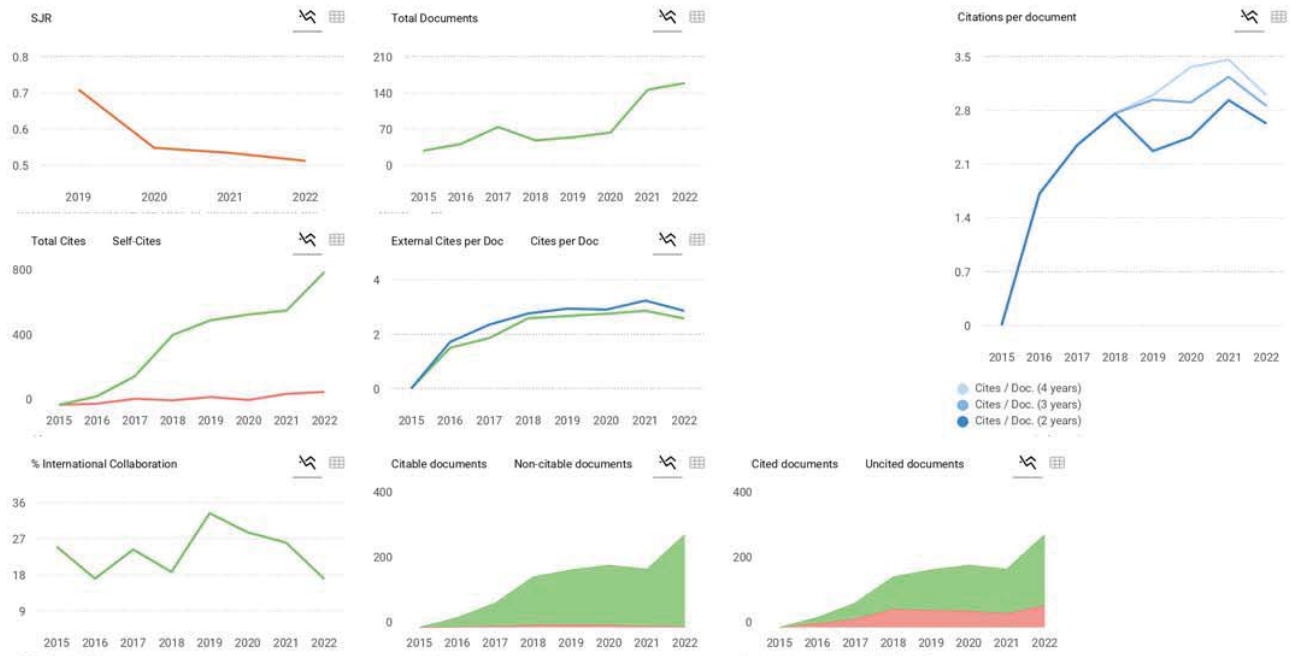
 Join the conversation about this journal

 Quartiles  


### FIND SIMILAR JOURNALS

options 

1 <b>Metallurgical Research and Technology</b> FRA  48% similarity	2 <b>Canadian Metallurgical Quarterly</b> GBR  47% similarity	3 <b>Mineral Processing and Extractive Metallurgy:</b> GBR  45% similarity	4 <b>World of Metallurgy - ERZMETALL</b> DEU  42% similarity	5 <b>Journal of Material Cycles and Waste Management</b> JPN  36% similarity
-------------------------------------------------------------------------------------------------------------------------------------------------------------------	--------------------------------------------------------------------------------------------------------------------------------------------------------------	---------------------------------------------------------------------------------------------------------------------------------------------------------------------------	---------------------------------------------------------------------------------------------------------------------------------------------------------------	-------------------------------------------------------------------------------------------------------------------------------------------------------------------------------



Journal of Sustainable Metallurgy

← Show this widget in your own website

Q2 Environmental Science (miscellaneous) best quartile

SJR 2022 0.51

powered by scimagojr.com

Just copy the code below and paste within your html code:

`<a href="https://www.scim.`

SCImago Graphica

Explore, visually communicate and make sense of data with our new data visualization tool.

Metrics based on Scopus® data as of April 2023

Leave a comment

Name

Email

(will not be published)

Submit

The users of Scimago Journal & Country Rank have the possibility to dialogue through comments linked to a specific journal. The purpose is to have a forum in which general doubts about the processes of publication in the journal, experiences and other issues derived from the publication of papers are resolved. For topics on particular articles, maintain the dialogue through the usual channels with your editor.

Developed by:



Powered by:



Follow us on @ScimagoJR

Scimago Lab, Copyright 2007-2022. Data Source: Scopus®

EST MODUS IN REBUS  
Version 1.0.0 (2022)

[Cookie settings](#)

[Cookie policy](#)

---





# Source details

## Journal of Sustainable Metallurgy

Scopus coverage years: from 2015 to 2023

Publisher: Springer Nature

ISSN: 2199-3823 E-ISSN: 2199-3831

Subject area: Materials Science: Metals and Alloys Environmental Science: Environmental Science (miscellaneous) Engineering: Mechanics of Materials

Source type: Journal

[View all documents >](#) [Set document alert](#) [Save to source list](#)

CiteScore 2022 **3.3** ⓘ

SJR 2022 **0.512** ⓘ

SNIP 2022 **1.007** ⓘ

[CiteScore](#) [CiteScore rank & trend](#) [Scopus content coverage](#)

CiteScore 2022 ▼

**3.3** =  $\frac{1,386 \text{ Citations } 2019 - 2022}{419 \text{ Documents } 2019 - 2022}$

Calculated on 05 May, 2023

CiteScoreTracker 2023 ⓘ

**4.0** =  $\frac{1,849 \text{ Citations to date}}{467 \text{ Documents to date}}$

Last updated on 05 December, 2023 • Updated monthly

### CiteScore rank 2022 ⓘ

Category	Rank	Percentile
Materials Science		
Metals and Alloys	#55/164	66th
Environmental Science		
Environmental Science (miscellaneous)	#63/163	61st
Engineering		

[View CiteScore methodology >](#) [CiteScore FAQ >](#) [Add CiteScore to your site ↗](#)

---

## About Scopus

[What is Scopus](#)

[Content coverage](#)

[Scopus blog](#)

[Scopus API](#)

[Privacy matters](#)

## Language

[日本語版を表示する](#)

[查看简体中文版本](#)

[查看繁體中文版本](#)

[Просмотр версии на русском языке](#)

## Customer Service

[Help](#)

[Tutorials](#)

[Contact us](#)

---

## ELSEVIER

[Terms and conditions](#) ↗ [Privacy policy](#) ↗

All content on this site: Copyright © 2024 Elsevier B.V. ↗, its licensors, and contributors. All rights are reserved, including those for text and data mining, AI training, and similar technologies. For all open access content, the Creative Commons licensing terms apply.

We use cookies to help provide and enhance our service and tailor content. By continuing, you agree to the use of cookies ↗.

